Search for Photoproduction of Bosons by the Missing-Mass Technique and Measurement of the s and t Distribution of the Photoproduced Hadronic Continuum*

Gary E. Gladding,† John J. Russell,‡
Michael J. Tannenbaum,§ Jeffrey M. Weiss,‖
and Gordon B. Thomson**
Harvard University, Cambridge, Massachusetts 02138
(Received 18 July 1973)

The reaction $\gamma + p \to p + m^0$ was studied with a tagged-photon beam of energy range 1.90 to 4.70 GeV. No new resonances were seen in the state m^0 but instead a large nonresonant production was observed. The s and t dependences of this continuum production were measured and found to have interesting properties. The recoil-proton spectra from the photoproduced continuum are found to strongly resemble recoil-proton spectra from hadron-initiated reactions.

I. INTRODUCTION

Although high-energy photon beams have been available for some years, no systematic survey with good mass resolution has been made of the energy and momentum-transfer dependence of hadronic photoproduction. Particular final states have been studied with most of the effort concentrated on observing the two-pion spectrum from the reaction $\gamma + p \to p + \pi^+ + \pi^-$.[1] Studies of more complicated final states have been made mainly in limited-statistics track-chamber experiments.[2] Another approach, first taken by a SLAC group,[3] studied particle production by measuring the recoil-proton spectrum from a bremsstrahlung beam using a statistical subtraction method to extract particle cross sections. We have improved on this by using a tagged-photon beam which enables the incident energy, momentum transfer, and the mass of the produced state to be determined directly for each individual event.

II. EXPERIMENTAL METHOD

We have measured the distribution of recoil protons produced in the reaction

$$\gamma + p \to p + X^0$$

by a tagged-photon beam. X^0 is any resonant or nonresonant hadronic final state against which the proton recoils and is described by an invariant mass m, which was experimentally determined by the missing-mass technique.

The tagged-photon beam was derived from the Cambridge Electron Accelerator (CEA) and had a resolution of 1.0% to 1.5% FWHM (full width at half maximum) for photon energies between 1.90 and 4.70 GeV (Fig. 1). A large-aperture magnetostrictive wire-chamber magnetic spectrometer was used to detect the recoil particles[4] (Fig. 2). The spectrometer had momentum resolution of $\pm 2\%$, which was largely determined by multiple scattering in the long air path. Separation of recoil protons from pions was accomplished by measurement of the time of flight of the particles in the spectrometer. The system had a measured time resolution of ± 0.8 nanosecond, which was sufficient to easily separate protons from pions up to a momentum of 1.13 GeV/c.

III. DATA COLLECTION AND ANALYSIS

The data reported here largely represent the second part of an experiment to survey the spectrum of photoproduced bosons in the mass range from 500 to 1700 MeV. The same apparatus was used in both parts of the experiment. In the first part of the experiment, previously reported,[5] the recoil spectrometer was positioned to accept particles with laboratory angles between 45 and 65 degrees, and the tagging system was adjusted for incident photon energies between 2.9 and 4.7 GeV. The resulting acceptance in missing mass from 500 to 1200 MeV was optimized for the detection of the well-known vector mesons ρ^0, ω^0, and ϕ^0.

For the data reported here, the angular acceptance of the recoil spectrometer was from 20 to 40 degrees with the incident-photon energy range from 1.90 to 4.70 GeV so as to perform a search for photoproduced bosons in the mass range from 900 to 1700 MeV. A total flux of 36.5×10^9 tagged photons was incident on a 24-inch-long liquid-hydrogen target and resulted in 675 000 triggers. Approximately one third of these triggers gave reconstructed trajectories in the spectrometer, and as in the first run,[5] half of these were pions and the rest protons. We eliminated roughly $\frac{3}{4}$ of the proton candidates in order to get clean geo-

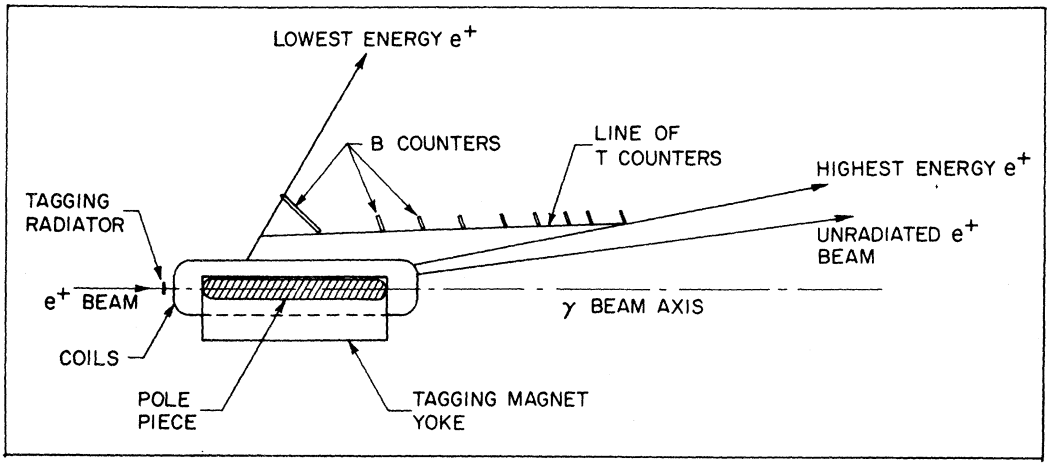

FIG. 1. CEA tagging system.

metrical cuts for the acceptance, and 24% of the remaining protons were eliminated as having been out of time with the tagged photon. This left 17 000 events, each of which could be uniquely specified by the three variables: k, the incident photon energy (or s, the total energy squared in the photon-proton center-of-mass system); t, the four-momentum transfer squared; and m, the missing mass. The average resolution in missing mass varied from 60 MeV FWHM at 650 MeV to 35 MeV FWHM at 1500 MeV. The resolution became worse as t increased and was dominated by the uncertainty in photon energy.

Because the acceptance of the apparatus varied significantly with m, t, and k and because our data were of rather high statistical quality, comparably accurate Monte Carlo calculations of the acceptance would have been unendurably time con-

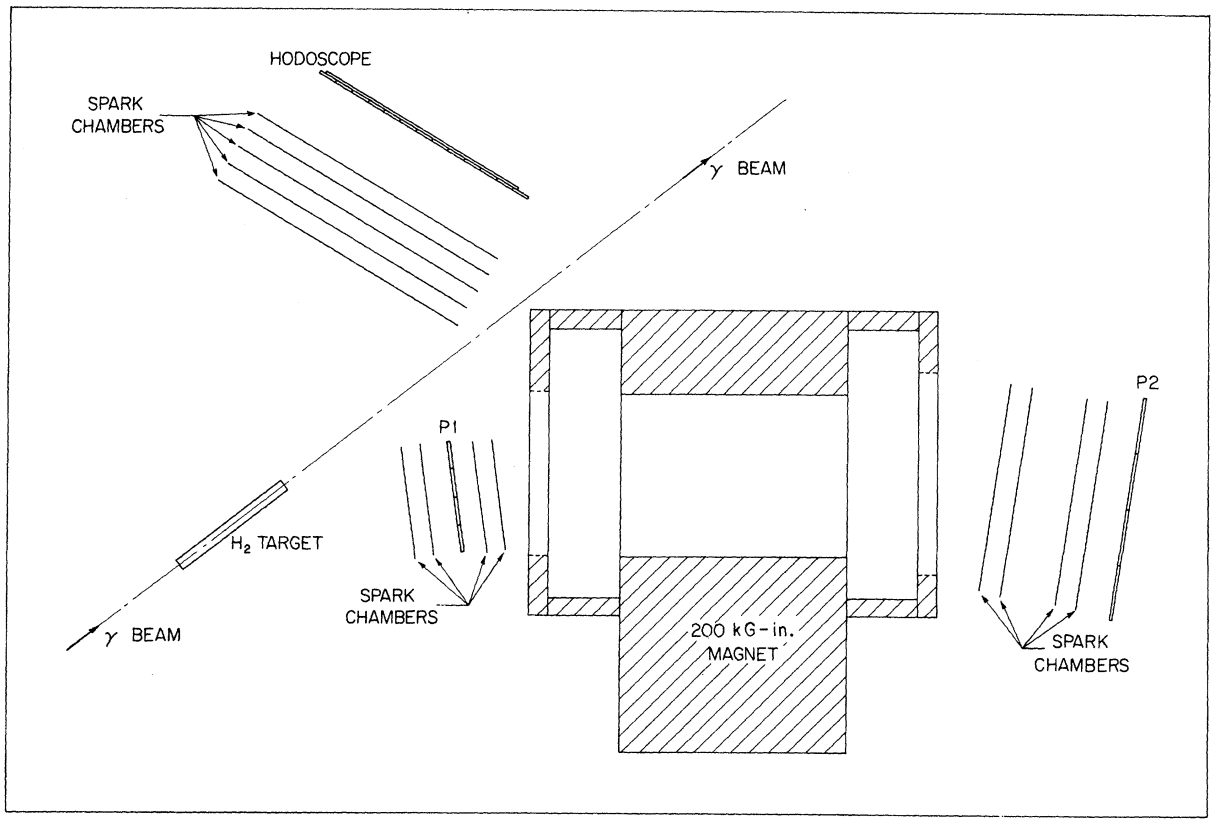

FIG. 2. Arrangement of magnetic spectrometer for high-mass run.

suming and inelegant. Hence, we made an analytical calculation of the acceptance for each event and used the inverse of the acceptance times flux to weight the individual event as it appeared in the various histograms. Thus, these histograms came out directly in units of cross section. The only subtlety in such a procedure is that the cuts on all the kinematic variables (s, t, m) must be chosen in such a way that the acceptance is never zero inside these cuts. In fact, we always chose our cuts so that the minimum acceptance was no less than one third of the maximum. The cuts were also made so that there was no correlation between t and m, i.e., each mass bin covered the same range in t.

The only correction required to the cross sections obtained in this manner was an over-all normalization correction of $(25.7 \pm 1.9)\%$, necessitating the raw cross sections to be corrected upwards by this amount. This can be broken down into a correction of $(14 \pm 1)\%$ for "spurious tagging," $(5.1 \pm 0.1)\%$ for tagging ambiguities, and $(4.5 \pm 1.5)\%$ for the time-of-flight ambiguities as explained in detail in our previous publication.[5]

IV. RESULTS

A. Missing-Mass Search

The result for the total missing-mass spectrum from both runs is shown in Fig. 3. The quantity plotted is the total cross section for missing-mass production in a 20-MeV-wide bin integrated over t

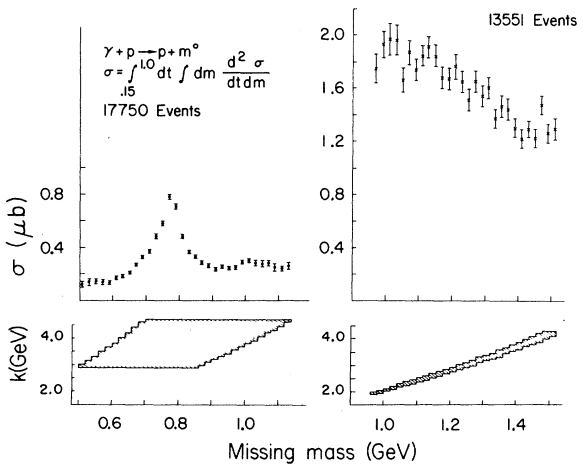

FIG. 3. Missing-mass distributions. The quantity plotted is the integral of the doubly differential cross section $d^2\sigma/dtdm$ over a 20-MeV mass bin and over t from 0.15 to 1.0 $(\mathrm{GeV}/c)^2$. For each 20 MeV mass bin, the photon energy is averaged over the interval given in the shaded insert. (a) Low-mass run: missing mass from 0.500 to 1.140 GeV. (b) High-mass run: missing mass from 0.980 to 1.520 GeV.

from $0.15 \leq t \leq 1.0$ $(\mathrm{GeV}/c)^2$ and averaged over an incident-photon energy range as shown in the shaded insert. Note that the acceptance in the high-mass run is relatively poor, in the sense that the missing mass observed is strongly correlated with the incident photon energy, while the acceptance of the low-mass run is good, in the sense that any photon energy can contribute to the average cross section over a large range in mass. The results obtained in the two runs are also quite different.

The low-mass run shows a clear peak due to the ρ^0 and ω^0 mesons, on top of a non-negligible background. Detailed results for the cross sections of these resonances have been previously given.[5] The high-mass run has no obvious resonant structure but is instead dominated by a continuum which is much larger in cross section than the ρ^0 or ω^0, and is several orders of magnitude larger than any ρ' resonances which have been reported[2,6] in the mass range 1000 to 1600 MeV. The region of missing mass from 1000 to 1100 MeV is also of particular interest since it is covered at different s in the two runs, and the cross sections observed are vastly different.

It is evident that the limits we can set for resonance photoproduction on top of this continuum will depend on the assumed width of the resonance. Our 40-MeV mass resolution will put any narrow resonance into two 20-MeV bins, whereas wide resonances will be essentially unaffected. Using the errors in each bin in Fig. 3, and the number of bins the assumed resonance would occupy, we can set upper limits for resonance production in this mass region as given in Table I.

Due to the presence of the large continuum, our limits for production of resonances are no better than those of previous experiments. However, our use of the tagged-photon technique enables us to measure some additional properties of this continuum.

TABLE I. 95%-confidence-level upper limits for the cross section of photoproduction of meson resonances. These limits apply to our observed cross section with $t > 0.15$ $(\mathrm{GeV}/c)^2$ and are not extrapolated to $t_{\min}$.

	95%-confidence-level observed-cross-section upper limit (μb)	
Mass (GeV)	Narrow (≤40 MeV)	Wide (120 MeV)
1.0	0.33	0.7
1.1	0.25	0.5
1.2	0.25	0.5
1.3	0.25	0.5
1.4	0.20	0.4
1.5	0.20	0.4

B. *s* and *t* Distribution of Continuum

While there have been extensive measurements of the *s* and *t* distributions of the well-known vector-meson resonances photoproduced in hydrogen, no measurements exist on the *s* and *t* dependence of the nonresonant 70—85% of the total cross section. We have studied the *s* and *t* dependence of this nonresonant production and have found structure in the *t* distributions of the continuum which was lacking in the mass spectrum.

The data can be characterized by three qualitative features. For any missing mass, the cross section falls off rapidly in *s*; the slope of the *t* distribution is independent of missing mass, but the slope shrinks linearly with increasing photon energy. This is best illustrated by the region of missing mass from 1.02 to 1.12 GeV, where data exist for two quite different incident energies in the two different runs.

Figure 4(a) gives the *t* distribution of the cross section for two different 20-MeV mass bins in the overlap region, each plotted for two different values of *s*. It is apparent that the high-energy points have a steeper slope as well as a lower intercept. Figure 4(b), on the other hand, gives two *t* distributions, each plotted at extreme values of missing mass for roughly the same value of *s*. Clearly the intercepts still fall with increasing *s*, but the slopes remain unchanged for the two distinct masses.

In order to study this strong *s* and *t* dependence of inclusive photoproduction in more detail, we rebin the data in 40-MeV-wide mass bins to be commensurate with our mass resolution. Then we eliminate the resonance region, $m < 1000$ MeV. Finally, we cut the data at higher *t* so that we can extend the acceptance of the high-mass run up to a mass of 1600 MeV at $s \cong 9.6$. The resulting set of data covers six mass bins from the low-mass run and 14 mass bins from the high-mass run, a total of 20 mass bins in each of which a spectrum was obtained for five intervals of *t*. There are two overlap regions in *m* and *s*: The mass region 1000 to 1100 MeV occurs at two values of *s*, 9.3 and 5.4 GeV^2; and an *s* of 8.75 GeV^2 occurs for two values of mass, 960 MeV and 1600 MeV.

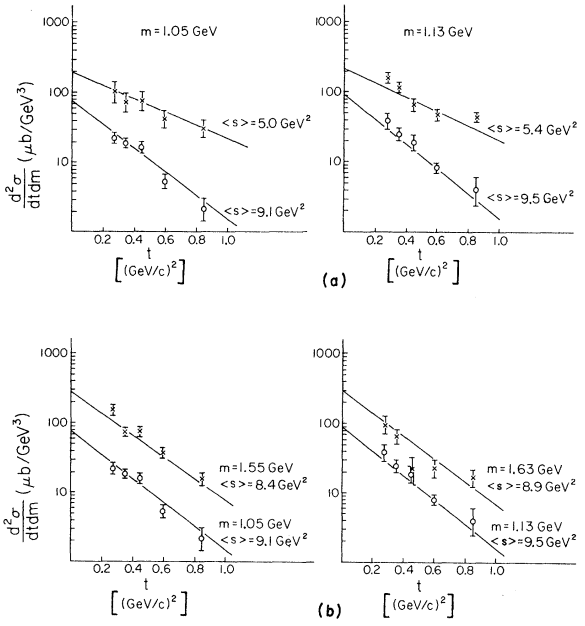

FIG. 4. (a) *t* distributions of the doubly differential cross section $d^2\sigma/dtdm$ for two 20-MeV mass intervals. Each plot shows data for two different *s* values. (b) *t* distributions at widely different values of missing mass but roughly the same values of *s*.

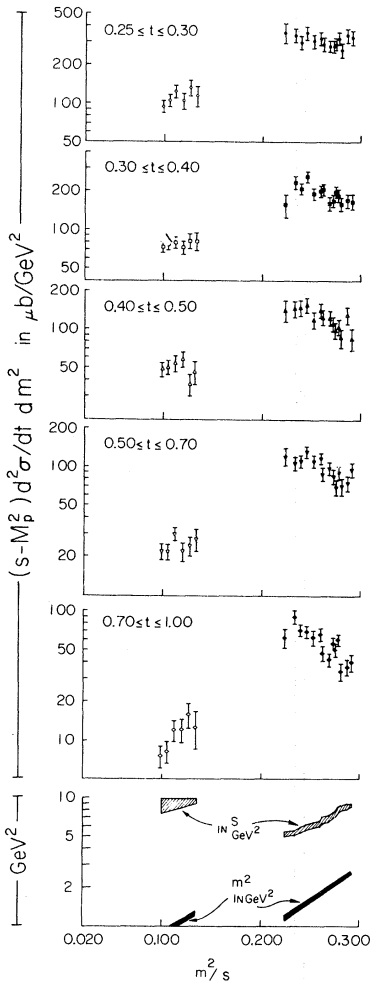

FIG. 5. The invariant cross section $(s - M_p^2)d^2\sigma/dtdm^2$ plotted against m^2/s for the five *t* intervals as labeled. Note that *s* and m^2 both vary to give the variation in m^2/s. The range of *s* and m^2 for each m^2/s bin is given at the bottom of the figure.

This is shown in Fig. 5, where the Lorentz-invariant inclusive cross section for recoil-proton production expressed in terms of t and missing mass $(s-M_p^2)d^2\sigma/dt\,dm^2$ is plotted against the scale-invariant quantity m^2/s. We chose this form so that the data at different energies and masses could all be put on the same graph. With the data plotted in this way, the large s dependence in the cross section for the mass range 1000 to 1100 MeV now manifests itself as a maximum near $m^2/s \cong 0.23$, which corresponds to an s of 5.3. The effect appears to increase with increasing t. There is also the distinct impression that a smooth curve could be fitted through all the data at a given value of s of about 8.5. We can then make use of the two overlap regions to separate the missing-mass dependence from the s dependence of the observed cross sections.

As we saw previously, the slopes as well as the intercepts at a given missing mass are strongly s-dependent; but at a fixed s there is no discernable dependence of the slope on missing mass. These properties can be summarized fitting all the data to the simple formula

$$(s-M_p^2)\frac{d^2\sigma}{d\,t\,dm^2} = A\left(\frac{m^2}{s}\right)^{\alpha} e^{-bst} ,$$

in which the linear shrinkage of the slope with s is manifest.

The best fit to the data is obtained with the parameters

$$A = 1635\ \mu\text{b/GeV}^2 ,$$

$$\alpha = 0.81 ,$$

$$b = 0.44\ \text{GeV}^{-4} ,$$

for s, t, and m^2 in units of GeV^2 and σ in units of μb, as shown in Fig. 4. The slopes are quite nondiffractive, ranging between 2.2 and 4.0 GeV^{-2}. The flatness of the slopes in this region was also observed by the DESY bubble chamber.[2] Note that this is not an acceptable fit to the data, having a χ^2 of 223 for 97 degrees of freedom. However, we present it because it captures all the features of the data with just three parameters.

A better fit was obtained with a sum of two exponential terms with coefficients having a common mass dependence but different s dependences, and exponents shrinking linearly with s:

$$\frac{d^2\sigma}{dtdm} = 1296\left(\frac{m^2}{M_p^2}\right)^{1.4} \times\left[\left(\frac{M_p^2}{s}\right)^{1.02} e^{-0.86st} + 2.7\left(\frac{M_p^2}{s}\right)^{2.5} e^{-0.20st}\right] \mu\text{b/GeV}^3 .$$

The χ^2 is 168 for 93 degrees of freedom, which is still not acceptable. The form of the fit is also rather awkward even though it was chosen for the fact that it best reproduced the properties of the data. Clearly, some appeal to the phenomenologists or to the results of other experiments is in order.

Regge-type analyses[7] simply do not work with our data since the observed linear shrinkage of the slope with s is quite incompatible with the Regge picture, which predicts a behavior of the form s to the power of t, or a logarithmic dependence of the slope on s:

$$\frac{d\sigma}{dt} \sim e^{-b\,\ln(s/m^2)t} .$$

However, the data do favor a saturation in the slope of the t distribution, as predicted by Leader and Pennington[8] for proton-proton elastic scattering. In fact, our data look very similar to the recoil-proton spectra observed in proton-proton inclusive reactions.

The only t distribution of recoil protons emerging from inelastic scattering of hadrons in the momentum-transfer range $0.4 \leq t \leq 0.7$ GeV^2 comes from a proton-proton experiment[9] at a single energy 28.5 GeV, and seems to show similar behavior to our t distributions, i.e., the slope is nondiffractive and does not depend much on missing mass. Because of the success of vector dominance and the quark model[3] in relating ρ^0 photoproduction to $\pi^{\pm}$ elastic scattering, we would also like to compare our recoil-proton spectra from continuum photoproduction with those from $\pi^{\pm}p$ inelastic scattering. Unfortunately, we could not find any such πp data in a form amenable to easy comparison. However, there are other pp data[10] plotted in the fashionable inclusive variables, and it turns out to be quite instructive to analyze our data in this form.

C. Inclusive Cross Sections

The Lorentz-invariant cross section for particle production in any reference frame is given by

$$E\frac{d^3\sigma}{dp^3} \equiv f(p_\perp, p_\parallel, s) ,$$

where $p_\perp$, $p_\parallel$, and E are the transverse momentum, longitudinal momentum, and energy of the particle in the reference frame. Evaluating d^3p in cylindrical coordinates, assuming azimuthal symmetry of the reaction, and defining the new variable

$$Q \equiv p_\perp^2 ,$$

we get the relations

$$d^3p = p_\perp dp_\perp dp_\parallel d\phi$$
$$= 2\pi p_\perp dp_\perp dp_\parallel$$
$$= \pi dQ\, dp_\parallel .$$

Defining x as the fraction of the possible center-of-mass longitudinal momentum of a particle,

$$x \equiv \frac{p^*_\parallel}{\sqrt{s}/2} = 2p^*_\parallel/\sqrt{s} ,$$

we can then relate the many different ways invariant cross sections are presented:

$$E\frac{d^3\sigma}{d^3p} = E^*\frac{d^3\sigma}{d^3p^*}$$
$$= \frac{E^*}{2\pi p^*_\perp}\frac{d^2\sigma}{dp^*_\perp dp^*_\parallel}$$
$$= \frac{2E^*}{\pi\sqrt{s}}\frac{d^2\sigma}{dxdQ} \equiv f(Q,x,s) .$$

In terms of the more conventional variables s, t, and m,

$$E\frac{d^3\sigma}{d^3p} = \frac{(s-M_p^2)}{\pi}\frac{d^2\sigma}{dt\,dm^2}$$

or

$$(s-M_p^2)\frac{d^2\sigma}{dtdm^2} = \pi f(Q,x,s) .$$

Many authors also use the noninvariant cross section

$$\frac{d^2\sigma}{dxdQ} = \frac{\pi\sqrt{s}}{2}\frac{d^3\sigma}{d^3p^*}$$
$$= \frac{\sqrt{s}}{2}\frac{d^2\sigma}{dp_\perp^2 dp^*_\parallel}$$
$$= \frac{\pi\sqrt{s}}{2E^*} f(Q,x,s) .$$

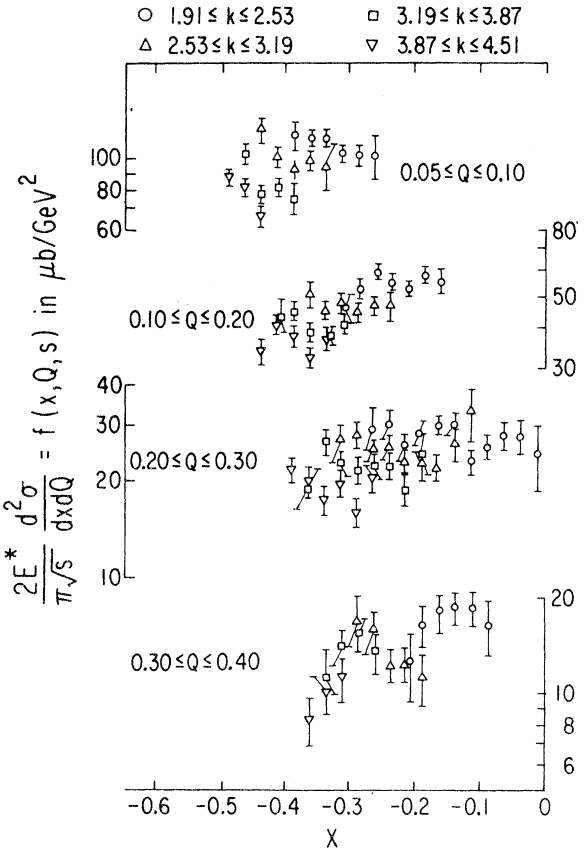

FIG. 6. The invariant cross section for inclusive proton photoproduction, $(2E^*/\pi\sqrt{s})d^2\sigma/dxdQ$. Distributions in x are given for four incident energy intervals and four ranges of $Q = p_\perp{}^2$ as indicated on the figure.

Converting our data to the inclusive variables is rather straightforward but not entirely trivial. It is not sufficient to simply use the Jacobian of the transformation since the bins in t and m do not map into square bins on the x,Q plane. The data must actually be rebinned in terms of the variables x and Q and then the kinematic cuts on x and Q must be chosen to ensure a region of good acceptance. This procedure is very important since the cross section has a precipitous dependence on the variable Q.

The results for the Lorentz-invariant cross sections expressed in inclusive variables $(2E^*/\pi\sqrt{s})\times d^2\sigma/dxdQ$ are shown in Fig. 6. These cross sections were obtained using only the data from the high-mass run. The "poor" acceptance again appears here as a strong correlation between x and s for a given Q.

At first glance, the photoproduction cross sections appear to differ qualitatively from the pp results. The outstanding characteristic of the inclusive proton spectrum from proton-proton collisions is that the noninvariant cross section $d^2\sigma/dxdQ$ is flat in x.[10,11] Our photoproduction cross sections are not flat in x but show a clear tendency to droop as x becomes more negative. However, the correlated acceptance prevents us from determining whether this is an x dependence or an s dependence or whether it is due to the factor $2E^*/\pi\sqrt{s}$.

We can try to eliminate these effects by concentrating on just one of our four photon energy bins in Fig. 6 and calculating the noninvariant cross section. As shown in Fig. 7(a), the noninvariant photoproduction cross section $d^2\sigma/dxdQ$ for the energy bin $3.19 \leq k \leq 3.87$ GeV is consistent with being flat in x, i.e., it resembles the hadron data.[10] Thus we can attempt to actually make a quantitative comparison between the γp and the pp data. In Fig. 7(a), with mean energy $\bar{k} = 3.52$ GeV

for the range $0.30 \leq Q \leq 0.40$ GeV^2 and x around -0.3, the noninvariant γp cross section is

$$\frac{d^2\sigma}{dx\,dQ} = 52 \pm 5\ \mu\text{b/GeV}^2 .$$

For the pp data, the fit given by Anderson *et al.*[10] at 30 GeV/c for the noninvariant cross section $d^2\sigma/dx\,dQ$ is consistent with the results of Allaby *et al.*[10] at 19.2 GeV/c and Abolins *et al.*[10] at 6.6 GeV/c in the range $0.3 < Q < 0.5$ GeV^2 if there is a momentum dependence of roughly $p^{-1/4}$, i.e.,

$$\frac{d^2\sigma_{pp}}{dx\,dQ} = \frac{2620}{p^{1/4}}\, p_\perp e^{-p_\perp/0.166}\ \text{mb/(GeV/}c)^2 ,$$

where p and $p_\perp$ are the incident momentum and outgoing transverse momentum in GeV/c. Using this formula, we find for the pp cross section at 3.52 GeV/c and the range $0.3 \leq Q \leq 0.4$ GeV^2

$$\frac{d^2\sigma}{dx\,dQ} = 32 \pm 1\ \text{mb/GeV}^2 .$$

This gives the ratio of the cross sections for inclusive recoil-proton production as

$$\frac{\sigma_{pp}}{\sigma_{\gamma p}} = 615 \pm 62 .$$

Making a crude attempt to use the quark model and vector dominance,[3] we can set

$$\frac{\sigma_{pp}}{\sigma_{\gamma p}} = \frac{\sigma_{pp}}{\sigma_{\pi p}}\,\frac{\sigma_{\pi p}}{\sigma_{pp}}\,\frac{\sigma_{\rho p}}{\sigma_{\gamma p}} = \frac{3}{2}\,\frac{\gamma_\rho^2/4\pi}{\alpha/4} = 822 \times \gamma_\rho^2/4\pi ,$$

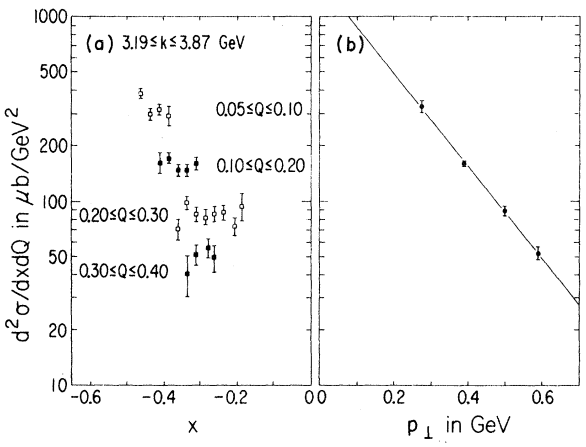

FIG. 7. The noninvariant cross section $d^2\sigma/dx dQ$ for recoil-proton photoproduction for the incident energy range $3.19 \leq k \leq 3.87$ GeV. (a) Distribution versus x for constant Q. (b) Transverse-momentum dependence obtained by assuming that the cross section is independent of x.

in which case we find

$$\gamma_\rho^2/4\pi = 0.75 \pm 0.08 .$$

Considering all the assumptions and extrapolations made, this result is in remarkably good agreement with the accepted value, as well as with the value of $\gamma_\rho^2/4\pi = 0.80 \pm 0.04$ obtained from our analysis[5] of the ρ^0 peak in the low-mass run [Fig. 3(a)]. Since the transverse momentum dependence observed in the photon data [Fig. 7(b)] is also nearly identical to the transverse momentum dependence of the pp data, it is clear that there really is a remarkable similarity between the recoil-proton spectra from photon-initiated inclusive reactions and those from proton-initiated reactions. Hence, it is also clear that the strong s and t dependence observed in the recoil-proton spectra from inclusive photoproduction is not just a fluke of photon physics but rather seems to be a general feature of inclusive reactions in the proton fragmentation region. As our photoproduction measurements cover a large range of s, t, and m^2 in the proton fragmentation region, we can try to use the data to study these general features of inclusive reactions in more detail.

D. n^2 Analysis

We had previously noted that the linear dependence of the slope of the t distributions on s, observed in our data, was incompatible with the Regge picture,[7] but was consistent with a saturation of the slope with increasing s as predicted by Leader and Pennington.[8] By introducing the variable n^2, the invariant length of the four-dimensional normal to the scattering plane, to replace t, the invariant four-momentum transfer, Leader and Pennington concluded that the slope shrinkage in real and quasi-two-body reactions would saturate according to the formula

$$d\sigma/dt \sim \exp\left[\beta_0 t\left(1 - \sum_{i=1}^{4} m_i^2/s\right)\right],$$

where β_0 is a constant and m_i, $i = 1,4$, are the masses of the two incident and two outgoing particles. Krisch[8] used a similar variable for pp elastic scattering. Another consequence of the n^2 analysis, conjectured by Leader and Pennington,[8] was that the invariant cross section when plotted as a function of n^2, s, and m^2 will turn out to be a function of n^2 only. Our data are also consistent with this remarkable property.

The four-vector n for the reaction $a+b \to c+d$ is given by

$$n_\mu = 2\epsilon_{\mu\nu\rho\sigma}\, p_a^\nu\, p_b^\rho\, p_c^\sigma/(p_a+p_b)^2 \ .$$

If particle b is a proton at rest, this reduces to the expression

$$n = (\vec{n}, i0)\,,$$

where the 3-vector $\vec{n}$ is

$$\vec{n} = \frac{2iM_p}{s}\ \vec{p}_a \times \vec{p}_c \ .$$

Thus for photoproduction of recoil protons from a proton at rest, we find

$$|n^2| = (1-M_p^2/s)^2\, p_\perp^2 \ ,$$

where $p_\perp$ is the transverse momentum of the recoil proton.

The removal of the s and m^2 dependence obtained by plotting the invariant cross section versus n^2 instead of t is shown in Fig. 8. In Fig. 8(a), we plot the invariant cross section

$$(s-M_p^2)\frac{d^2\sigma}{dtdm^2}$$

versus t for three mass bins from the overlap region of Fig. 5, two bins of the same mass squared of 1.25 GeV^2 at widely different s of 5.4 and 9.3 GeV^2, and a third bin of roughly the same s of 8.5 GeV^2 but with a much higher missing mass squared of 2.43 GeV^2. As mentioned previously (Fig. 4), the slopes as well as the intercepts at a given missing mass are strongly s-dependent,

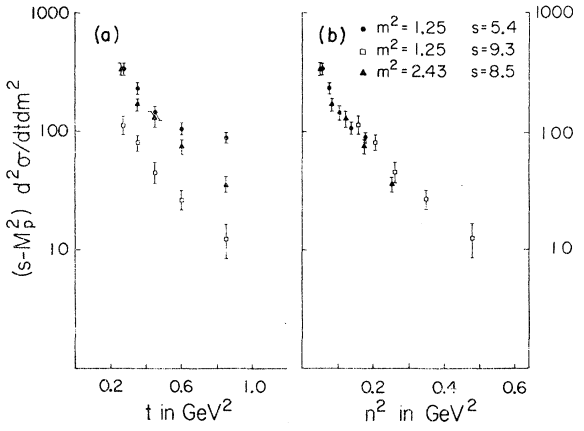

FIG. 8. The Lorentz-invariant cross section $(s-M_p^2)d^2\sigma/dtdm^2$ plotted against the invariant four-momentum transfer t and the invariant length of the four-dimensional normal to the scattering plane n^2 for the same three 40-MeV-wide mass bins in the overlap region: Two bins of the same mass squared of 1.25 GeV^2 at widely different s of 5.4 and 9.3 GeV^2; and the third bin of roughly the same s of 8.5 GeV^2 but with a much higher mass squared of 2.43 GeV^2. (a) t distribution; (b) n^2 distribution.

but at fixed s there is no discernible mass dependence of the slope. Figure 8(b) shows the same invariant cross section for the same three mass bins given in Fig. 8(a), this time plotted against n^2. Now all the points appear to lie on a universal curve.

If we take all the data points from Fig. 5 and plot them against n^2, we still get a universal curve which appears to be a function of n^2 only (Fig. 9). The data can be fitted either as the sum of two exponentials in n^2:

$$(s-M_p^2)\, d^2\sigma/dtdm^2 = 1200\ e^{-44n^2} + 260\, e^{-6.7n^2}$$

or by the simpler form

$$(s-M_p^2)\, d^2\sigma/dtdm^2 = 17.5\ \frac{e^{-5.0n^2}}{n^2}\ \mu\text{b/GeV}^2 \ ,$$

both of which give χ^2 of 180 for 97 degrees of freedom. The fit is still not acceptable but could be made so if we allowed a 15% absolute normalization discrepancy between the high-mass and the low-mass runs.

It is also possible that the tendency of the data from the high-mass run to lie consistently 15% higher than the data from the low-mass run is a real physical effect which cannot simply be dismissed as a normalization error. As we have no independent check of the relative normalization of the two runs, the only other course open to us is to try to find a dependence of the n^2 distribution on any of the other physical variables.

Since n^2 is related to $p_\perp^2$, the transverse mo-

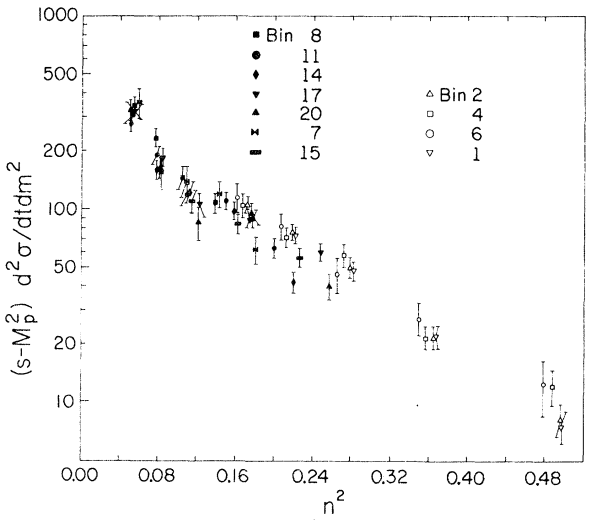

FIG. 9. The invariant cross section $(s-M_p^2)d^2\sigma/dt\,dm^2$ vs n^2 for the same data points in Fig. 5. For clarity, only half the points are plotted. The bin numbers refer to the mass bins from Fig. 5, numbered from left to right.

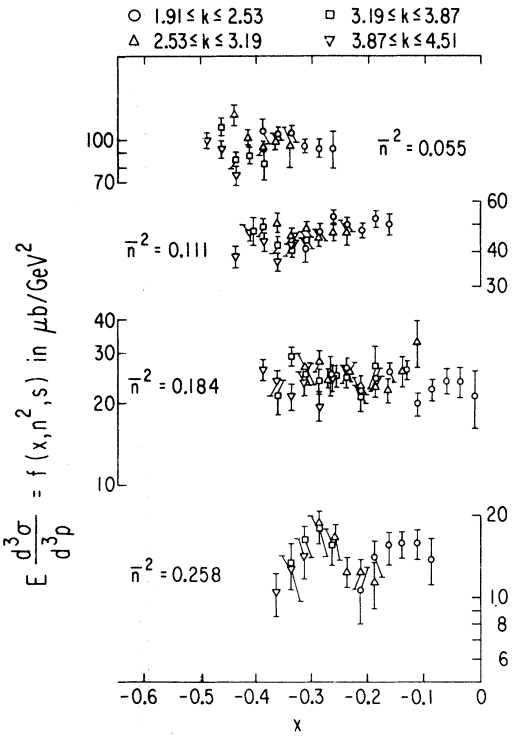

FIG. 10. The invariant cross section for inclusive proton photoproduction $E^*d^3\sigma/d^3p^*$, plotted versus x for fixed values of n^2. The data points are the same as Fig. 6 except that they have been extrapolated from a constant value of Q to a constant value of n^2 by using the n^2 fit given in the text.

mentum, the most logical other physical to try is the longitudinal momentum, or x. Figure 10 shows the invariant cross section

$$E^*\frac{d^3\sigma}{d^3p^*}$$

plotted versus x for fixed values of n^2. This figure was obtained by taking the data from Fig. 6 and using the above fit in n^2 to extrapolate all the points at a given value of Q and different values of s to the same value of n^2. Clearly, the x distribution of the invariant cross section at constant values of n^2 (Fig. 10) is much flatter than the χ distribution at constant $p_\perp^2$ (Fig. 6), and could even be construed to have absolutely no dependence on x. In any case, it is certainly true that analyzing the invariant cross section in terms of the variable n^2 greatly simplifies and perhaps even eliminates entirely the dependence of the cross section on other physical variables.

V. CONCLUSIONS

The results presented here show that to 95% confidence level there are no resonances of mass 1.10 to 1.50 GeV, and width 120 MeV or less, photoproduced with cross section as much as 0.5 μb for $t > 0.15$ (GeV/c)^2. This implies that the total hadronic photoproduction cross section consists mostly of a continuum of incoherent multiparticle final states. Our measurements of the recoil-proton spectra from photoproduction in hydrogen, for the incident energy range 1.90 to 4.70 GeV, show that the 80–85% of the total photon cross section which is nonresonant has a definite momentum-transfer and energy dependence which is vastly different from that of the diffractive production of vector mesons, which provides the other 15–20% of the total cross section. The momentum-transfer dependence of the recoil-proton spectrum from continuum photoproduction in the range $0.15 \leq t \leq 1.0$ GeV^2 is rather nondiffractive, does not depend much on missing mass, but does shrink strongly with increasing photon energy. In fact, the properties of inclusive recoil-proton spectra from photoproduction are remarkably similar to those of inclusive proton spectra produced in hadron-proton collisions. Analysis of the invariant cross section for inclusive recoil-proton photoproduction in terms of the variable $n^2 = (1 - M_p^2/s)^2 \times p_\perp^2$ seems to greatly simplify and perhaps even eliminate entirely the dependence of the cross section on other physical variables.

*Work supported by U. S. Atomic Energy Commission under Contract Nos. AT(30-1)-2752 and AT(11-1)2232.

†Present address: University of Illinois, Champaign-Urbana, Illinois 61801.
‡Present address: Southeastern Massachusetts University, North Dartmouth, Massachusetts 02747.
§Present address: The Rockefeller University, New York, New York 10021. Alfred P. Sloan Foundation Fellow.
‖Present address: CERN, 1211 Geneva 23, Switzerland.
**Present address: Case Western Reserve University, Cleveland, Ohio 44106.

[1]N. Hicks *et al.*, Phys. Lett. 29B, 602 (1969); G. McClellan *et al.*, Phys. Rev. Lett. 23, 718 (1969); F. Bulos *et al.*, *ibid.* 26, 149 (1971); H. Alvensleben *et al.*, *ibid.* 26, 273 (1971).
[2]M. Davier *et al.*, Phys. Rev. D 1, 790 (1970); J. Ballam, *ibid.* 5, 545 (1972); Aachen-Berlin-Bonn-Hamburg-Heidelberg-München Collaboration, Phys. Rev. 188, 2060 (1969); Y. Eisenberg *et al.*, Phys. Rev. Lett. 22, 669 (1969).
[3]R. Anderson, D. Gustavson, J. Johnson, D. Ritson, B. H. Wiik, W. G. Jones, D. Kreinick, F. Murphy, and R. Weinstein, Phys. Rev. D 1, 27 (1970).
[4]Details of the apparatus can be found in the following Harvard theses: Gary Earle Gladding, 1971 (unpub-

lished); Jeffrey Martin Weiss, 1972 (unpublished); and Gordon Bennett Thomson, 1972 (unpublished).
[5]G. E. Gladding, J. J. Russell, M. J. Tannenbaum, J. M. Weiss, and G. B. Thomson, preceding paper, Phys. Rev. D 8, 3721 (1973).
[6]H. H. Bingham *et al.*, Phys. Lett. 41B, 635 (1972); G. Bacci *et al.*, *ibid.* 38B, 551 (1972); G. Barbarino *et al.*, Nuovo Cimento Lett. 3, 689 (1972).
[7]C. E. DeTar *et al.*, Phys. Rev. Lett. 26, 675 (1971); J. M. Wang and L. L. Wang, *ibid.* 26, 1287 (1971); S. D. Ellis and A. I. Sanda, Phys. Lett. 41B, 87 (1972).
[8]E. Leader and M. R. Pennington, Phys. Rev. Lett. 27, 1325 (1971); A. D. Krisch, *ibid.* 19, 1149 (1967); E. Leader and M. R. Pennington, Phys. Rev. D 7, 2668 (1973).
[9]W. E. Ellis, R. R. Kinsey, T. W. Morris, R. S. Panvini, and F. Turkot, Phys. Lett. 32B, 641 (1970).
[10]J. Allaby *et al.*, CERN Report No. CERN-70-12 (unpublished); M. A. Abolins *et al.*, Phys. Rev. Lett. 25, 126 (1970); E. W. Anderson *et al.*, *ibid.* 19, 198 (1967).
[11]R. C. Hwa, Phys. Rev. Lett. 26, 1143 (1971).

PHYSICAL REVIEW D VOLUME 8, NUMBER 11 1 DECEMBER 1973

Study of the η' Meson from the Reaction $K^-p \to \Lambda\eta'$ at 2.18 GeV/c *

Jerome S. Danburg,† George R. Kalbfleisch, Samuel R. Borenstein,‡
Richard C. Strand, and Vance VanderBurg
Brookhaven National Laboratory, Upton, New York 11973

J. W. Chapman, Richard K. Kiang,§ and J. Lys||
University of Michigan, Ann Arbor, Michigan 48104

(Received 27 June 1973)

We present new data on the η' meson based on 1414 η' events obtained from a 1 100 000-picture exposure of the BNL 31-inch hydrogen bubble chamber to a 2.18-GeV/c K^- beam. We have measured the η' mass, width, and branching ratios. We find that the very-forward-produced η' mesons have anisotropic angular distributions with respect to the incident K^- beam, suggesting that possibly $J^{PC} = 2^{-+}$; however, the standard Dalitz-plot analyses favor $J^{PC} = 0^{-+}$ over 2^{-+}.

I. INTRODUCTION

We report a study of the η' meson decaying into the modes (1) $\pi^+\pi^-\eta_N$, (2) $\pi^+\pi^-\eta_C$, (3) $\pi^+\pi^-\gamma$, and (4) all neutrals. The subscripts N and C refer to the η-decay modes $\eta \to$ neutrals and $\eta \to \pi^+\pi^-\pi^0$, $\pi^+\pi^-\gamma$, respectively. This study is based on 1.1 $\times 10^6$ pictures (approximately 40 events/μb) of the hydrogen-filled 31-inch BNL bubble chamber, with an admixture of 4-mole-percent neon. The chamber was exposed to a 2.18-GeV/c K^- beam at the Brookhaven AGS in three runs.

The η' was discovered in 1964[1] and has been the subject of a number of subsequent investigations.[2-7]

The η' is known to be produced preferentially at low t (momentum transfer squared) in the reaction $K^-p \to \Lambda\eta'$,[1] and the scanning instructions for this experiment take advantage of this fact. Only events with a low-energy Λ decaying visibly into $p\pi^-$ are selected and this limits the scanning to unbiased events in which the momentum transfer squared from the target proton to the Λ is less than $\approx$0.8 GeV^2 in magnitude. In the analysis below we have imposed the more restrictive cut $|t| < 0.7$ GeV^2; this reduces the η' signal very little. Some preliminary results based on about 85% of the data have been reported previously.[8]

II. SELECTION OF EVENTS

A. The Final States $\Lambda\pi^+\pi^-\eta_N$, $\Lambda\pi^+\pi^-$ MM (for the Decays $\eta' \to \pi^+\pi^-\eta_N$, $\pi^0\pi^0\eta_C$)

The final-state assignment $\Lambda\pi^+\pi^-\eta_N$ means a successful fit with the mass of the missing neutral system equal to that of the η; MM means a missing neutral system with missing mass greater than two π^0 masses. Figure 1(a) is a plot of the mass recoiling against the Λ vs the unfitted missing-mass squared; it contains 4025 events. Only one of the interpretations $\Lambda\pi^+\pi^-\eta_N$, $\Lambda\pi^+\pi^-$MM is used per event, and if both are possible, only $\Lambda\pi^+\pi^-\eta_N$ is used. In the case of $\Lambda\pi^+\pi^-\eta_N$, the abscissa shows the *fitted* $\pi^+\pi^-\eta_N$ mass; the ordinate always is the unfitted MM^2. The cluster near the middle of this plot contains about 650 events and is evidence of the final state $\Lambda\eta'$, $\eta' \to \pi^+\pi^-\eta_N$; almost all the events in the cluster have a fit to $\Lambda\pi^+\pi^-\eta_N$. Fig-